Widespread readthrough events in plants reveal unprecedented plasticity of stop codons

Yuqian Zhang[1,2,6], Hehuan Li[1,6], Yanting Shen[3,6], Shunxi Wang[1], Lei Tian[1], Haoqiang Yin[1], Jiawei Shi[1], Anqi Xing[4], Jinghua Zhang[1], Usman Ali[1], Abdul Sami[1], Xueyan Chen[1], Chenxuan Gao[1], Yangtao Zhao[1], Yajing Lyu[1], Xiaoxu Wang[1], Yanhui Chen[1], Zhixi Tian[3,5,*], Shu-Biao Wu[2,*], Liuji Wu[1,2,*]

[1] National Key Laboratory of Wheat and Maize Crop Science, Collaborative Innovation Center of Henan Grain Crops, College of Agronomy, Henan Agricultural University, Zhengzhou, China.

[2] School of Environmental and Rural Science, University of New England, Armidale, NSW, Australia.

[3] State Key Laboratory of Plant Cell and Chromosome Engineering, Institute of Genetics and Developmental Biology, Chinese Academy of Sciences, Beijing, China.

[4] Department of Plant and Environmental Sciences, Clemson University, Clemson, SC, USA.

[5] College of Advanced Agriculture Sciences, University of Chinese Academy of Sciences, Beijing, China.

[6] These authors contributed equally.

***Corresponding authors**

Zhixi Tian (zxtian@genetics.ac.cn), Shu-Biao Wu (shubiao.wu@une.edu.au), and Liuji Wu (wlj200120@163.com)

Abstract

Stop codon readthrough (SCR), the decoding of a stop codon as a sense codon by the ribosome, has important biological implications but remains largely uncharacterized in plants. Here, we identified 1,009 SCR events in two monocots (maize, rice) and two dicots (soybean, *Arabidopsis*) using a proteogenomic strategy with 80 customized databases. SCR transcripts were mostly significantly shorter and had fewer components than non-SCR transcripts in two monocot plants, although these differences were not as significant in the dicots. Mass spectrometry evidence revealed that all three stop codons involved in SCR events could be recoded as 20 standard amino acids, some of which were also supported by suppressor transfer RNA analysis. In addition, we observed multiple functional signals in the C-terminal extensions of 34 maize SCR proteins, and characterized the structural and subcellular localization changes in the extended protein of BASIC TRANSCRIPTION FACTOR 3. Overall, our study not only demonstrates that SCR events are widespread in plants but also reveals the unprecedented recoding plasticity of stop codons, which provides important new insights into the flexibility of genetic decoding.

Introduction

The rules of the genetic code were long considered universal dogma in all organisms after the standard genetic code was deciphered decades ago. However, exceptions to the rules have been increasingly observed in different species over the years, substantially altering the perception of the decoding rules from being static to dynamic[1,2]. Living organisms are now widely understood to employ various modes to expand the coding potential of their genome, such as alternative translation initiation[3], ribosome frameshifting[4], and translational bypassing[5]. Stop codon readthrough (SCR) is another important means of recoding that is classified as a non-canonical translational event[6,7]. SCR occurs when the ribosome reads a stop codon (UGA, UAG, or UAA) as a sense codon rather than the stop signal with the translation terminating at a later in-frame stop codon[7,8]. Such an event can generate a C-terminally extended protein isoform which may acquire novel biological functions, since the amino acid sequence appended at the C-terminus possibly alters the activity[9], stability[10], and/or subcellular localization[2,11] of the protein. Indeed, SCR proteins have been implicated in a variety of biological processes, such as the regulation of intercellular cytoplasm flow[12], neuronal integrity and reproductive health[13], cellular redox homeostasis[2,14], and angiogenesis[15,16].

Initially discovered in viruses as a strategy to expand protein-coding potential[17-19], SCR was subsequently identified in other organisms. In plant pathogens, *Phosphoglycerate kinase* (*PGK*) in *Ustilago maydis* and *Glyceraldehyde-3-phosphate dehydrogenase* (*GAPDH*) in *Aspergillus nidulans* are typical functional readthrough genes conserved in fungal species[2]. In the yeast *Saccharomyces cerevisiae*, the [PSI+] strain forms prion-like polymers of the abnormal eukaryotic release factor 3 (eRF3), which is implicated in translation termination and peptide release, resulting in a high level of readthrough across many genes[20], including *Phosphodiesterase 2* (*PDE2*), *Interacting with mpp10p 3* (*IMP3*), and *Bypass of stop codon 4* (*BSC4*)[10,21,22]. In *Drosophila melanogaster*, readthrough is estimated to affect over 300 genes[23,24], such as *kelch* (*kel*)[12,25], *Synapsin* (*Syn*)[26], *headcase* (*hdc*)[27], and *traffic jam* (*tj*)[13]. In

mammals, *Hemoglobin beta chain* (*HBB*)[28], *Myelin protein zero* (*MPZ*)[29], *Vascular endothelial growth factor-A* (*VEGF-A*)[15], *Mitochondrial carrier 2* (*MTCH2*)[30], *Argonaute 1* (*AGO1*)[31], *Opioid related nociceptin receptor 1* (*OPRL1*)[32], *Mitogen-activated protein kinase 10* (*MAPK10*)[32], *Aquaporin 4* (*AQP4*)[33], *Lactate dehydrogenase B* (*LDHB*)[34], *Malate dehydrogenase 1* (*MDH1*)[34], *Vitamin D receptor* (*VDR*)[35], and *Adenosylmethionine decarboxylase 1* (*AMD1*)[36,37] have been confirmed to undergo readthrough. However, SCR events in plants remain largely uncharacterized, with only one study reporting 144 readthrough genes in *Arabidopsis* detected with ribosome profiling[38]. Therefore, further exploration of SCR events with a more robust analysis is warranted in a wide range of plant species.

It is crucial to identify the amino acids decoded at the stop codon sites, as they can strongly affect the functionality of readthrough protein isoforms[11,21,39]. Previous studies have shown that UGA could be translated to arginine, asparagine, cysteine, glutamine, glycine, serine, threonine, tryptophan, and tyrosine[30,31,39-41]; UAA to alanine, glutamate, glutamine, lysine, serine, tryptophan, and tyrosine[39,42-45]; and UAG to alanine, arginine, aspartate, glutamate, glutamine, glycine, leucine, lysine, serine, threonine, tryptophan, tyrosine, and valine[30,39,46,47]. However, knowledge about the amino acids translated at stop codon sites in SCR events remains unknown in Plantae. In addition, the potential for stop codons to be recoded as amino acids other than those reported above has not been investigated yet.

Here, we employed a mass spectrometry (MS)-based proteogenomic strategy to study SCR events in plants and to identify the amino acids at the readthrough stop codon sites. We detected a total of 1,009 SCR events in the monocots maize and rice, and dicots soybean and *Arabidopsis*, and characterized their features. Interestingly, we discovered that the three stop codons could be recoded as all 20 standard amino acids, which reveals the unprecedented recoding plasticity of stop codons and the dynamic nature of genetic decoding. We also delineated the first comprehensive landscape of SCR events in plants at the protein level, uncovering a collection of previously unknown readthrough proteins to further explore their biological functions.

98 # Results

99 ## A proteogenomic strategy to identify SCR events in plants

100 The SCR event is a means of alternative translation by redefining UGA, UAG, or
101 UAA to specify amino acids, thus extending the translation at the C-terminus. The
102 most definitive evidence for SCR occurrence is the direct detection of translation at
103 the stop codon sites. However, SCR events are non-canonical and cannot be identified
104 by a typical proteomic strategy. Therefore, we implemented a proteogenomic strategy
105 integrating MS-based proteomics with 20 customized databases to identify SCR
106 events in maize at the protein level (Fig. 1). First, total protein was extracted from
107 maize leaves, followed by digestion, fractionation, and liquid chromatography-tandem
108 mass spectrometry (LC-MS/MS) analysis to obtain MS/MS datasets of peptides for
109 subsequent identification. We then constructed 20 customized databases with in-house
110 scripts as described in the Methods section.

111 To capture SCR events in maize, we used the obtained MS/MS data to search
112 against the 20 SCR customized databases with MaxQuant search engine. This strategy
113 identified 708 unique "through" peptides spanning the stop codon site. For further
114 quality control of MS data, we next applied more stringent criteria for "through"
115 peptides to identify SCR events with high confidence (see Methods). The screening
116 steps resulted in much more reliable "through" peptides, which corresponded to 367
117 SCR events involving 1,063 proteins (Supplementary Table 1). All identified peptides
118 for SCR proteins are listed in Supplementary Table 2. Collectively, these results not
119 only demonstrate the abundance of readthrough events naturally occurring in maize,
120 but also uncover a previously unknown source of protein isoforms produced by SCR.

121 ## Verifying SCR events in maize

122 To verify the SCR events in maize identified above, we retrieved the available
123 ribosome profiling (Ribo-seq) datasets of 56 maize samples from NCBI to analyze the
124 SCR events at the mRNA level. Four Ribo-seq datasets with higher quality were
125 finally retained after further screening (see Methods). We then analyzed the three-

126 nucleotide (3-nt) periodicity of the Ribo-seq reads (30-mers) in the coding sequences
127 (CDSs), putative extensions, and distal 3′ untranslated regions (UTRs). The results
128 showed that the putative extensions exhibited a visible hallmark of 3-nt periodicity (P
129 < 0.05, Fig. 2a), i.e., the reading frame 0 occurred significantly higher than the other
130 two, which was similar to that of the CDSs (Fig. 2a). By contrast, such difference was
131 not observed in the distal 3′ UTRs (Fig. 2a). In addition, the average ribosome
132 footprint density (in RPKM) of putative extensions was significantly higher than that
133 of the distal 3′ UTRs in the four datasets ($P < 0.001$, Fig. 2b). These results suggest
134 that readthrough is a significant contributor to the ribosome footprint density in
135 putative extensions. After applying the conditions described in the Methods section
136 for the four Ribo-seq datasets to verify SCR, we found that 55 out of the 367 SCR
137 events identified by the proteogenomic approach were also corroborated by Ribo-seq
138 analysis (Fig. 2c and Supplementary Table 3).

139 We selected two SCR representative genes, *ZmH3C2* and *ZmCEQORH*, which
140 exerted functional roles in distinct biological processes related to chromatin assembly
141 and stress response, respectively, for further analysis. For *ZmH3C2*, which encodes
142 HISTONE H3.2, MS analysis identified the readthrough peptide AAAAGRPDRPWR
143 with its second alanine (A) translated at the UAG site (Fig. 2d and Supplementary Fig.
144 1a). The readthrough of this gene was also evidenced by ribosome footprints within
145 the extended region downstream of the annotated stop codon (Fig. 2e). For
146 *ZmCEQORH*, encoding CHLOROPLAST ENVELOPE QUINONE
147 OXIDOREDUCTASE, MS analysis identified the "through" peptide
148 AQEVWAKSIDGHATGKIVVEMGGAAEETR, in which the antepenultimate
149 glutamate (E) was incorporated at the UGA site (Fig. 2h and Supplementary Fig. 1b).
150 We also observed ribosome footprints beyond the annotated stop codon of the
151 corresponding transcript (Fig. 2i).

152 In addition, we performed *in vitro* translation experiments using wheat germ
153 extract to further demonstrate the readthrough of the above two genes. The results
154 showed that *ZmH3C2* and *ZmCEQORH* had significantly higher readthrough

155 activities compared to the SCR-negative gene *Zm00001d009138* ($P < 0.001$), as
156 demonstrated by the detection of luciferase activities. The SCR rates of *ZmH3C2* and
157 *ZmCEQORH* were 12% and 5%, respectively (Fig. 2f, j). It is known that the rate of
158 the basal translation error is lower than 0.1%[8], thus the results indicate that *ZmH3C2*
159 and *ZmCEQORH* underwent the programmed SCR events. Further MS analysis of the
160 readthrough products identified the "through" peptides AAAAGRPDRPWR and
161 GGAAEETR for the two genes, where the UAG and UGA were recoded as alanine
162 and glutamate (Fig. 2g, k), respectively. Taken together, our Ribo-seq analysis, *in vitro*
163 translation experiments, and MS analysis validated the SCR events identified using
164 proteogenomics in maize, and demonstrated the feasibility of the proteogenomic
165 method for large-scale identification of SCR events in plants.

166 Characteristics of SCR events in maize

167 To understand the characteristics of SCR events in maize, we first analyzed the stop
168 codon preferences. All three stop codons were read through among the 367 SCR
169 events: UGA was involved in 174 events (47.4%), followed by UAG in 102 events
170 (27.8%) and UAA in the remaining 91 events (24.8%) (Fig. 3a). We found that UGA
171 was the most frequent next in-frame stop codon following these readthrough stop
172 codons, accounting for 76 cases after the readthrough UGA, 46 cases after the
173 readthrough UAG, and 40 cases after the readthrough UAA (Fig. 3a). The genome-
174 wide distribution pattern showed that these SCR events were distributed
175 heterogeneously across each chromosome of maize, and many of the SCR events were
176 closer to the telomeres (Fig. 3b). In addition, a collection of 379 hotspot regions were
177 obtained, 244 of which were SCR hotspot regions while 135 were non-SCR hotspot
178 regions (Fig. 3b). These results revealed the wide distribution of SCR events in the
179 maize genome.

180 Furthermore, we compared the length and complexity of SCR and non-SCR
181 transcripts. Interestingly, we observed that the SCR primary transcripts were
182 significantly shorter than the non-SCR transcripts (Fig. 3c). The average lengths of
183 the elements from the primary transcripts, including coding sequences (CDSs), introns,

184 and 3′ UTRs, were also markedly shorter in SCR events than those in non-SCR events
185 (Fig. 3c). The 5′ UTR was also shorter in readthrough transcripts, albeit not
186 statistically significant. Consistent with the length of readthrough transcripts, their
187 corresponding proteins had notably shorter lengths with fewer amino acids
188 (Supplementary Fig. 2a) and lower molecular weight (Supplementary Fig. 2b).
189 Moreover, SCR primary transcripts had significantly fewer exons (Fig. 3d) and splice
190 variants (Fig. 3e) than those of non-SCR primary transcripts.

191 Earlier studies have shown that *cis*-acting elements such as nucleotides
192 immediately surrounding the readthrough stop codon and motifs downstream the stop
193 codon can influence readthrough[48-50]. We thus examined the local mRNA context of
194 SCR transcripts. An analysis of nucleotide frequencies in positions adjacent to the
195 readthrough stop codons showed a bias of A>U>C>G at the -2 position, A>G>C>U at
196 the -1 position, A>G>U>C at the +4 position, and U>C>G>A at the +5 position
197 (Supplementary Fig. 3a). The most frequent tetranucleotide pattern (stop codon plus
198 the following nucleotide) was UGA-U (Supplementary Fig. 3b). Extended regions
199 downstream of the annotated stop codons in the readthrough transcripts were enriched
200 with featured sequence motifs (Supplementary Dataset 1). Three motif examples,
201 ZNF263, ASCL1, and ETV6 are shown in Supplementary Fig. 3c. These motifs
202 enriched in extended regions likely exert effects on the particular facets of SCR by
203 interacting with specific proteins. In addition, extended regions of SCR transcripts
204 harbored remarkably lower free energy than their analogs of non-SCR transcripts
205 (Supplementary Fig. 3d), suggesting more stable secondary structures in the
206 extensions of the readthrough transcripts.

207 Stop codons are recoded as 20 amino acids in maize SCR events

208 Since translation of the stop codon is crucial for SCR events, we examined which
209 amino acids were translated at every readthrough stop codon site based on the MS
210 data. Quite unexpectedly, we found that, with the exception of UAA which was
211 recoded to 19 amino acids (except serine), UGA and UAG were translated to all 20
212 standard amino acids in maize SCR events (Fig. 4a). Among all the amino acids,

213 glutamate was the most recoded amino acid for UGA (in 17 SCR events, 8.9%),
214 methionine for UAG (in 17 cases, 15.6%), and aspartate for UAA (in 11 cases, 11.6%).
215 Previous literature has reported several amino acids that were able to be
216 translated at stop codon sites in different species (Fig. 4b and Supplementary Table 5),
217 prompting us to explore the reasons behind the recoding plasticity of the stop codons
218 in our results. Suppressor transfer RNA s (tRNAs) are specific tRNA species forming
219 classical base pairing with the stop codon, which can lead to the translation[24]. We thus
220 conducted a genome-wide search for such potential suppressor tRNAs capable of
221 reading stop codons in maize by running tRNAscan-SE[51] and ARAGORN[52]. As a
222 result, we acquired a collection of UGA-, UAG-, and UAA-recognizing tRNAs.
223 Multiple sequence alignments of the predicted suppressor tRNAs against the NCBI
224 Nucleotide (NT) database resulted in different groups of suppressor tRNAs well
225 aligned with the canonical tRNAs of a range of amino acids (Supplementary Table 6).
226 We identified six classes of UGA suppressor tRNAs (Supplementary Tables 5 and 6):
227 $tRNA^{Met}$(UCA), $tRNA^{Lys}$(UCA), $tRNA^{Val}$(UCA), $tRNA^{Gly}$(UCA), $tRNA^{Ile}$(UCA), and
228 $tRNA^{Thr}$(UCA). The predicted secondary structures of the first two UGA suppressor
229 tRNAs are shown in Fig. 4c I, II, and their nucleotide sequence alignments are
230 presented in Supplementary Fig. 4a, b. We also detected six classes of UAG
231 suppressor tRNAs (Supplementary Tables 5 and 6): $tRNA^{Glu}$(CUA) (Fig. 4c III and
232 Supplementary Fig. 5a), $tRNA^{Trp}$(CUA) (Fig. 4c IV and Supplementary Fig. 5b),
233 $tRNA^{Arg}$(CUA), $tRNA^{Asp}$(CUA), $tRNA^{Gly}$(CUA), and $tRNA^{Lys}$(CUA). Furthermore,
234 we identified eight classes of UAA suppressor tRNAs (Supplementary Tables 5 and 6):
235 $tRNA^{Lys}$(UUA) (Fig. 4c V and Supplementary Fig. 6a), $tRNA^{His}$(UUA) (Fig. 4c VI
236 and Supplementary Fig. 6b), $tRNA^{Ala}$(UUA), $tRNA^{Asn}$(UUA), $tRNA^{Gly}$(UUA),
237 $tRNA^{Phe}$(UUA), $tRNA^{Met}$(UUA), and $tRNA^{Thr}$(UUA). Collectively, the suppressor
238 tRNAs identified in maize provide potential reasons for the translation of at least
239 some amino acids at stop codon sites.

240 SCR events and recoding plasticity of stop codons in other plants

241 In light of the abundant SCR events identified in maize, we questioned if SCR also

occurred in other plant species. We thus followed the same proteogenomic method with the respective 20 custom databases to explore SCR events in rice, soybean, and *Arabidopsis*. Indeed, we detected abundant SCR events in these species with similar features to those in maize. We identified 198 SCR events in rice (Supplementary Table 7), 179 SCR events in soybean (Supplementary Table 9), and 265 SCR events in *Arabidopsis* (Supplementary Table 11), corresponding to 269, 385, and 468 proteins, respectively.

In rice, we observed that the stop codon usage SCR events was in the order of UGA > UAA > UAG, and the next in-frame stop codon following the readthrough stop codons also displayed a preference for UGA (Fig. 5a). For the dicots soybean and *Arabidopsis*, the stop codon usages were the same in the order of UGA > UAA > UAG in SCR events, while the most frequent next in-frame stop codon after the readthrough stop codons was UGA for soybean and UAA for *Arabidopsis* (Fig. 5b, c). Genome-wide distribution analysis showed that SCR events were distributed across all chromosomes in their respective plant species (Fig. 5d, e, f). We also analyzed the features of SCR and non-SCR transcripts in the three plants. In rice, the length of SCR primary transcripts and transcript elements including CDSs, introns and the 5′ UTR were shorter than those of non-SCRs ($P < 0.05$, Supplementary Fig. 7a, b). In addition, the SCR primary transcripts tended to possess fewer exons (Supplementary Fig. 7c) and had significantly fewer splice variants ($P < 0.001$, Supplementary Fig. 7d) than non-SCR transcripts. In the dicots soybean and *Arabidopsis*, however, the SCR transcript features were not apparent as compared to those in monocots. SCR transcripts in soybean had significantly shorter UTR lengths and fewer exons than the non-SCR transcripts ($P < 0.05$, Supplementary Fig. 8b, c) but no significance for other feature comparison (Supplementary Fig. 8a, b, d). Similarly, SCR transcripts from *Arabidopsis* showed no significant different from the non-SCR counterparts except fewer splice variants (Supplementary Fig. 9a, b, c, d).

Analysis of the recoded amino acids at stop codon sites revealed that UGA exhibited great plasticity to be recoded as the 20 standard amino acids in all the three

271 plant species (Fig. 5g, h, i). For UAG, it was recoded to 18 amino acids (except serine
272 and tryptophan) in rice (Fig. 5g), 17 amino acids (except cystine, aspartate, and
273 phenylalanine) in soybean (Fig. 5h), and 18 amino acids (except aspartate and
274 arginine) in *Arabidopsis* (Fig. 5i). Similarly, UAA was translated to 17, 16, and 20
275 amino acids in rice, soybean, and *Arabidopsis*, respectively (Fig. 5g, h, i). These
276 results further uncover the high recoding plasticity of stop codons in plant SCR events.

277 C-terminal extensions in maize SCR events contain multiple 278 functional signals

279 To examine the biological implications of SCR events, we searched the functional
280 signals in all C-terminal extensions of readthrough proteins in maize. As a result,
281 multiple functional signals were detected in 34 extensions, including the
282 transmembrane domains in 28 extensions, nuclear localization signals in two
283 extensions, and peroxisomal targeting signals (PTS1) in four extensions (Fig. 6a and
284 Supplementary Table 13). Among them, we selected BASIC TRANSCRIPTION
285 FACTOR 3 (ZmBTF3), which was predicted to possess a transmembrane domain in
286 its C-terminal extension (54 amino acids), for further analysis. First, we conducted the
287 *in vitro* translation experiment to validate the readthrough of this gene. We observed
288 high readthrough activity of *ZmBTF3* with an SCR rate of 15% (Fig. 6b), which
289 revealed that *ZmBTF3* was read through and generated a novel isoform (hereafter
290 termed ZmBTF3x). Next, we confirmed the expression of the fusion protein
291 ZmBTF3x-Fluc by immunoblotting using an anti-Fluc antibody (Fig. 6c). The results
292 showed that the molecular weight of the readthrough protein ZmBTF3x-Fluc was the
293 same as its positive control ZmBTF3x^{ACA}-Fluc and higher than that of ZmBTF3-Fluc
294 (Fig. 6c). By contrast, no visible band of readthrough products expressed from the
295 SCR-negative control *Zm00001d009138-TAG-ISR-Fluc* was observed in the
296 immunoblot (Fig. 6c). The fusion protein ZmBTF3x-Fluc was then subjected to mass
297 spectrometric analysis, resulting in the detection of different types of peptides labeled
298 as "before", "through", and "after", which further validated the production of the
299 readthrough protein isoform ZmBTF3x (Fig. 6d, top). The spectrum for "through"

300 peptide "EPEEKKESTFCCV" revealed that the stop codon UAA was translated as
301 threonine (T) (Fig. 6d, bottom).

302 The single transmembrane domain predicted in the C-terminus of ZmBTF3x was
303 found to contain 20 amino acid residues crossing the membrane (Fig. 6e). The
304 predicted 3D structures of ZmBTF3 and ZmBTF3x revealed an α-helix appended at
305 the ZmBTF3x C-terminus that was not present in ZmBTF3 (Fig. 6f). Furthermore, the
306 α-helix with a high pLDDT score and low PAE score corresponded exactly to the
307 region of the predicted transmembrane domain (Fig. 6f and Supplementary Fig. 10a,
308 b). To examine the biological significance of the C-terminal extension derived from
309 SCR of *ZmBTF3*, we constructed *35S:ZmBTF3-GFP* and *35S:ZmBTF3x-GFP* vectors
310 and individually transfected them in maize protoplasts for subcellular localization
311 analysis using confocal microscopy. The results showed that ZmBTF3 localized to the
312 nucleus and cytosol (Fig. 6g), consistent with the previous study reporting that
313 *Arabidopsis* BTF3 acted as the transcription factor and the β-subunit of nascent
314 polypeptide-associated complex (NAC)[53]. By contrast, the readthrough protein
315 ZmBTF3x localized to the plasma membrane and cytosol (Fig. 6g), confirming the
316 localization change between the isoforms ZmBTF3 and ZmBTF3x. In summary, these
317 results indicate that SCR can lead to the structural and subcellular localization change
318 of the readthrough protein isoform, which may confer new biological functions.

319 Discussion

320 SCR, classified as the recoding of stop codons, is a regulatory mode of translation that
321 could produce multiple protein isoforms from the same transcript[1,54]. SCR has been
322 reported in a variety of organisms with important biological implications. Recently,
323 Sahoo *et al*. have identified mRNAs of 144 genes that exhibited SCR in *Arabidopsis*
324 by analyzing Ribo-seq datasets[38]. However, a systematic study of SCR events in
325 plants at the protein level is still lacking. In the current study, we employed a high-
326 resolution MS-based proteogenomic strategy to analyze SCR events in different plants
327 and to identify the amino acids translated at stop codon sites. We established 20
328 customized databases for each of the four plant species, which enabled detection of

329 any potential SCR events with all possible amino acids translated at stop codon sites.
330 Using this strategy, we detected 1,009 SCR events corresponding to a collection of
331 2,185 proteins in four plant species.

332 Our systematic analysis of SCR events revealed their similar characteristics
333 among the four plant species. Firstly, SCR events occur in all chromosomes of the
334 four species, and SCR events are prone to be dispersively distributed in the
335 chromosome, except in maize where the higher distribution of SCR was closer to
336 telomeres. Secondly, consistent with previous studies[6,23], UGA is the most preferential
337 stop codon for readthrough, and it also turned out to be the most preferred next in-
338 frame stop codon in SCR events of these species. In addition, SCR transcripts were
339 mostly significantly shorter and had fewer exons and splice variants than non-SCR
340 transcripts in two monocot plants, although these were not as significant as that in the
341 dicots. However, in other eukaryotes like *D. melanogaster* and *Anopheles gambiae*,
342 SCR transcripts were found to be much longer than the non-SCR transcripts, possibly
343 because the occurrence of SCR requires more regulatory elements embedded in their
344 longer transcripts[23,24]. Our findings suggest that the regulation of SCR in plants might
345 differ from that in animals.

346 The stop codons are able to be recoded as all 20 standard amino acids in the four
347 plant species in our study, which has not been reported elsewhere. This result suggests
348 a greater recoding potential of stop codons underestimated in the past and reveals a
349 more flexible mode of decoding. Since tRNA is the adapter molecule in decoding a
350 codon to an amino acid, we explored the reasons for the plasticity of stop codons by
351 tRNA analysis. Suppressor tRNAs, of which the anti-codon could fully form
352 canonical base-pairing with stop codons, have been reported to contribute to the
353 translation of stop codons[24,55,56]. Here, we detected an array of suppressor tRNAs
354 corresponding to different amino acids in maize, which may be the underlying reasons
355 for the translation of six amino acids at UGA, six amino acids at UAG, and eight
356 amino acids at UAA sites. In addition to suppressor tRNAs, near-cognate tRNAs of
357 stop codons are also an important reason for the translation due to the noncanonical

358 base pairing of one position between a stop codon and the anticodon of the tRNA[41,44].
359 The amino acids carried by these near-cognate tRNAs include arginine, serine,
360 tryptophan, cysteine, glycine, and leucine for UGA; lysine, glutamate, glutamine,
361 tryptophan, serine, leucine, and tyrosine for UAG; and lysine, glutamate, glutamine,
362 tyrosine, serine, and leucine for UAA[57,58]. However, we did not find suppressor
363 tRNAs for the rest small portion of the 20 amino acids recoded at stop codon sites in
364 our study, nor the tRNAs of these amino acids were near-cognate tRNAs (e.g., the
365 case of UAG recoded as alanine and UGA recoded as glutamate in Fig. 2). Indeed,
366 these amino acids are not exclusively observed in this study, as previous studies have
367 also reported some of their translation at stop codon sites[15,30,39,46]. These cases suggest
368 that our present understanding of stop codon reading by suppressor or near-cognate
369 tRNAs is still incomplete. Considering the sophisticated modifications and regulation
370 of the decoding adaptor tRNAs and multiple factors that influence SCR events[8,59], the
371 mechanism underlying SCR associated with different tRNAs warrants further study.

372 In summary, we implemented a proteogenomic strategy and identified abundant
373 SCR events across the genomes of four plant species. Stop codons in these SCR
374 events could be recoded as all 20 standard amino acids. We demonstrated that SCR
375 events are widespread in plant species and uncovered the unprecedented plasticity of
376 stop codons. Our findings provide evidence that genetic decoding is far more flexible
377 than has been recognized. We also identified a large volume of novel protein isoforms
378 derived from SCR, which not only expands the plant proteome but also lays a
379 foundation for further exploring the functionality of SCR products.

380 # Methods

381 ## Sample preparation

382 Maize (*Zea mays,* B73 inbred line), rice (*Oryza sativa* L. ssp. *japonica* cv.
383 Nipponbare), *Arabidopsis thaliana* (Columbia-0), and soybean (*Glycine max* L.,
384 ZH13) plants were grown in a temperature- and light-controlled greenhouse. The
385 growth conditions for maize were a 15-h light/9-h dark photoperiod and a 28/25 °C
386 day/night air temperature, and samples were collected at the three-leaf stage. For rice,

387 the growth conditions were a 12-h light/12-h dark photoperiod and a 28/25 °C
388 day/night air temperature, and samples were collected on day 56. *Arabidopsis* plants
389 were grown in a greenhouse under a 16-h light/8-h dark photoperiod and a 22/21 °C
390 day/night air temperature, and samples were collected on day 21. Soybean plants were
391 grown in a greenhouse under a 16-h light/8-h dark photoperiod and a 22/21 °C
392 day/night air temperature, until the trifoliate leaves were fully expanded. Three
393 replicates of leaf samples for each of the plant species were harvested, frozen in liquid
394 nitrogen, and stored at –80 °C until analysis.

395 **Protein extraction**

396 Total proteins from each sample were extracted as previously reported[60]. Briefly, leaf
397 tissues (1 g) for each plant species were pulverized in liquid nitrogen, and the powder
398 was precipitated in 10% (w/v) trichloroacetic acid/acetone solution containing 65 mM
399 dithiothreitol (DTT) at –20 °C for 1 h. Then, the solution was centrifuged at 10,000×g
400 at 4 °C for 45 min and the supernatant was removed. The precipitate was then
401 vacuum-dried and solubilized in 1/10 volumes of SDT buffer (4% [w/v] SDS, 100
402 mM DTT, and 150 mM Tris-HCl, pH 8.0). After a 3-min incubation in boiling water,
403 the suspensions were ultrasonicated (80 w, ultrasonic 10 s/time, every 15 s, repeated
404 10 times) and incubated at 100 °C for 3 min. The extract was centrifuged at 12,000×g
405 at 25 °C for 10 min, and the total protein contents were quantified using BCA Protein
406 Assay Reagent (Promega Corporation). The supernatants were stored at –80 °C until
407 subsequent analysis.

408 **Protein digestion and peptide fractionation**

409 The total proteins (250 μg for each sample) were digested by FASP procedure using
410 trypsin (Promega Corporation) as described previously[60]. Then, the digested peptide
411 filtrate was fractionated by strong cation exchange (SCX) chromatography using an
412 AKTA Purifier system (GE Healthcare). The dried peptide mixture was reconstituted
413 and acidified with 2 ml buffer A (10 mM KH_2PO_4 in 25%[v/v] of ACN, pH = 2.7) and
414 loaded onto a PolySULFOETHYL 4.6×100 mm column (5 μm, 200 Å, PolyLC Inc).
415 The peptides were eluted at a flow rate of 1 ml/min buffer B (500 mM KCl, 10 mM

416 KH_2PO_4 in 25% of ACN, pH 2.7) in a gradient of 0-10% (v/v) for 2 min, 10-20% (v/v)
417 for 25 min, 20-45% (v/v) for 5 min, and 50-100% (v/v) for 5 min. The elution was
418 monitored by absorbance at 214 nm, and fractions were collected every 1 min. The 30
419 collected fractions were combined into 15 pools and desalted on C18 Cartridges
420 (Empore SPE Cartridges C18 standard density, bed I.D. 7 mm, volume 3 ml, Sigma-
421 Aldrich). Each fraction was concentrated by vacuum centrifugation and reconstituted
422 in 40 μl of 0.1% (v/v) trifluoroacetic acid. All samples were stored at –80 °C before
423 LC-MS/MS analysis.

424 **Liquid chromatography-tandem mass spectrometry analysis**

425 The samples were analyzed on a Q-Exactive HF-X mass spectrometer coupled to the
426 Easy nLC 1200 (Thermo Fisher Scientific). Peptide (2 μg) was loaded onto a 25 cm,
427 75 μm inner diameter C18-reversed phase column packed with 3 μm resin (EASY-
428 Column Capillary Columns, Thermo Fisher Scientific) in buffer A (2% [v/v]
429 acetonitrile and 0.1% [v/v] formic acid) and separated with a linear gradient of buffer
430 B (80% [v/v] acetonitrile and 0.1% formic acid) at a flow rate of 250 nl/min
431 controlled by IntelliFlow technology over 90 min. MS data were acquired using a
432 data-dependent top 10 method dynamically choosing the most abundant precursor
433 ions from the survey scan (m/z 300-1,800) for higher-energy collision dissociation
434 fragmentation (HCD). Determination of the target value was based on predictive
435 Automatic Gain Control (pAGC). The dynamic exclusion duration was 25 s. Survey
436 scans were acquired at a resolution of 70,000 (m/z 200), and the resolution for HCD
437 spectra was set to 17,500 (m/z 200). Normalized collision energy was 30 eV, and the
438 underfill ratio, which specifies the minimum percentage of the target value likely to
439 be reached at maximum fill time, was defined as 0.1%. The instrument was run with
440 peptide recognition mode enabled. MS experiments for each sample were conducted
441 in triplicate for each sample.

442 **Customized database construction**

443 The complete genome sequences of the four plants were downloaded from Ensembl
444 Plants (ftp://ftp.ensemblgenomes.org/pub/plants/release-41/fasta/zea_mays/dna/) for

445 maize, MSU Rice Genome Annotation Project
446 (http://rice.uga.edu/pub/data/Eukaryotic_Projects/o_sativa/annotation_dbs/pseudomol
447 ecules/version_7.0/all.dir/) for rice, the National Genomics Data Center
448 (ftp://download.big.ac.cn/gwh/Plants/Glycine_max_Gmax_ZH13_v2.0_GWHAAEV
449 00000000.1/GWHAAEV00000000.1.genome.fasta.gz) for soybean, and TAIR 10
450 (ftp://ftp.ensemblgenomes.org/pub/plants/release-
451 28/fasta/Arabidopsis_thaliana/dna/Arabidopsis_thaliana.TAIR10.28.dna.toplevel.fa.gz)
452 for *Arabidopsis* in FASTA format. The 20 customized databases for each plant species
453 were constructed as previously described with modifications[46].

454 **Identification of SCR events by MaxQuant**

455 The raw data were analyzed using MaxQuant software (v.1.6.1.10)[61]. The spectra
456 were searched against the 20 customized databases for each of the four plant species.
457 The initial search was set at a precursor mass window of 6 ppm. The search followed
458 an enzymatic cleavage rule of trypsin and allowed a maximum of two missed
459 cleavage sites and a mass tolerance of 20 ppm for fragment ions.
460 Carbamidomethylation of cysteines was defined as fixed modification, while
461 methionine oxidation was defined as variable modification for database searching.
462 The cutoff of global FDR for peptide and protein identification was set to 0.01.
463 Protein quantification was calculated by normalized spectral protein intensity.

464 All matched peptides were then relocated to the corresponding positions of
465 protein sequences in the reference databases and mapped to their genomic locations.
466 Every stop codon site was given an ID for genomic position recognition. The non-
467 redundant peptides uniquely mapped to the regions spanning the annotated stop codon
468 were labeled as "through", the peptides mapped to the coding sequence (CDS) region
469 were labeled as "before", and the peptides mapped to the 3′ UTR were labeled as
470 "after". We further implemented more stringent criteria to determine the “through”
471 peptides so as to identify SCR events. Only the unique “through” peptides that met the
472 following conditions were retained: (1) presented in at least two of the three replicates
473 in MS experiment; (2) at least two of the quality scores were higher than 20. Finally,

474 proteins sharing one stop codon site and containing a unique "through" peptide were
475 merged into one group and the group was defined as one SCR event.

476 **Ribosome profiling analysis**

477 We obtained ribosome profiling (Ribo-seq) datasets of 56 maize samples from
478 previous reports for SCR event analyzing[62-66]. The Ribo-seq data was analyzed
479 according to the methods described by Dunn et al. (2013)[11] and Sapkota et al. (2019)[6]
480 with modifications. Briefly, the ribosomal sequencing data were quality-controlled
481 using fastax (v.36.06) or cutadapt (v.1.13)[62] to remove low-quality bases, adaptor
482 sequences, and random primers. Reads of 25-35 nucleotides (nts) were retained by
483 seqkit (v.0.5.4) for subsequent analysis. The remaining reads were aligned to the
484 maize genome by STAR (v.2.7.3a)[67]. Ribosome-protected footprint alignments were
485 mapped to their estimated P-sites as follows: 12 nt were cut from each end of the
486 alignment, resulting in a fragment of $n \times$ nt in length ($n = l$-12×2). Each genomic
487 position covered by a nucleotide remaining in the truncated alignment was then
488 incremented by $1/n$ (count number). Then, the reads were mapped to the following
489 positions: 12 nts after the start codon, 15 nts before and 9 nts after the first stop codon,
490 and 15 nts after the second stop codon. This resulted in four regions remaining in the
491 transcripts: the 5′ UTR, CDS, readthrough region, and the distal 3′ UTR.

492 We then analyzed the length distribution of Ribo-seq reads in each dataset. Four
493 Ribo-seq datasets in which the read length was mainly distributed in 30-nt (30-mer)
494 and prepared with RNase I (little cutting bias) were finally retained for further SCR
495 validation. For analysis of 3-nt periodicity (phasing) of footprints, R package
496 ribosomeProfilingQC (v.1.10.0) was used and only 30-nt RPFs were counted, as
497 shown in maize with good-phased footprint population[62]. Reads were then counted in
498 all putative extended regions. Mean value of normalized RPKM (reads per kilobase
499 per million mapped reads) was calculated in R (v.3.2.5) in the four datasets. The
500 ribosome footprint density of putative extensions and the distal 3′ UTRs were
501 calculated in RPKM. Only extensions with RPKM > 1, read coverage > 10%, and no
502 overlap with any annotated 5′ UTRs, CDSs, and other non-coding RNAs were

503 retained and regarded as readthrough. Full data of samples that exhibited readthrough
504 in Ribo-seq analysis for each of the SCR events are shown in Supplementary Table 3.

505 **Distribution of readthrough events at the genomic level**

506 The genome-wide density of SCR and non-SCR events in maize chromosomes was
507 plotted using a sliding window of 20 Mb with 2-Mb steps according to the annotated
508 maize genome in Ensembl (https://plants.ensembl.org/index.html). We used "hotspot
509 region" to reflect the distribution density of SCR and non-SCR events. Hotspot
510 regions were defined as ≥ 5 SCR events for SCR hotspots and ≥ 335 for non-SCR
511 events in a window size of 20 Mb. The chromosomal distributions of rice SCR and
512 non-SCR events were drawn using a window size of 4 Mb with a step of 400 kb based
513 on the annotated rice genome from MSU (http://rice.uga.edu/). The same distribution
514 pattern was plotted with a window size of 10 Mb with a 1-Mb step based on the ZH13
515 reference genome (https://ngdc.cncb.ac.cn/gwh/Assembly/652/show) for soybean. For
516 *Arabidopsis*, the SCR and non-SCR genomic localizations were obtained by a 1.2-Mb
517 sliding window with a step size of 100 kb according to the annotated *Arabidopsis*
518 genome in TAIR (https://www.Arabidopsis.org/). Hotspot regions were defined as ≥3
519 for SCR events and ≥178 for non-SCR events in a window size of 4 Mb for rice, ≥2
520 for SCR events and ≥253 for non-SCR events in a window size of 10 Mb for soybean,
521 and ≥4 for SCR events and ≥157 for non-SCR events in a window size of 1.2 Mb for
522 *Arabidopsis*.

523 **Motif and minimum free energy analysis in readthrough regions of SCR**
524 **transcripts in maize**

525 Transcription factor-binding motifs in readthrough regions of maize SCR transcripts
526 were identified using the MEME-ChIP webserver (v.5.4.1)[68], and the annotations of
527 the obtained motifs were searched against the available databases for comparison
528 using Tomtom (v.5.0.5) with default parameters[69].

529 The minimum free energy of readthrough regions for maize SCR transcripts and
530 the comparable length between the first and downstream second stop codons for non-
531 readthrough transcripts were calculated using ViennaRNA Package (v.2.0) as

532 described[70].

533 **Identification and alignment of suppressor tRNAs in maize**

534 The complete maize genome sequences were downloaded from the Ensembl database
535 (ftp://ftp.ensemblgenomes.org/pub/plants/release-41/fasta/zea_mays/dna/). A genome-
536 wide search for suppressor tRNA genes was conducted using tRNAscan-SE (v.2.0)[51]
537 with default settings and ARAGORN[52] with both default settings and 0.95 default
538 settings as a lower scoring threshold. This analysis generated a collection of
539 suppressor/suppressor-like tRNAs recognizing the three stop codons from each search.
540 Comparison of the canonical tRNAs from different species with these predicted
541 suppressor tRNAs was performed using BLASTn (v.2.5.0+) against the NCBI
542 GenBank nucleotide (NCBI NT) database as previously described[55,56]. The potential
543 identity of the suppressor tRNAs corresponding to different amino acids could be
544 predicted from the high similarity of the sequence alignment between the suppressor
545 tRNAs and the canonical tRNAs of the standard amino acids.

546 **Motif and structure prediction of SCR proteins in maize**

547 C-terminal extensions at least 20 amino acids in length in maize SCR events were
548 scanned for transmembrane helices using TMHMM (v.2.0)[71] with default settings and
549 for nuclear localization signals using cNLS mapper[72]. C-terminal extensions at least
550 12 amino acids in length were searched for peroxisomal targeting signals using PTS1
551 Predictor[73] and prenylation signals using PrePS[74]. The 3D structures of ZmBTF3 and
552 ZmBTF3x were predicted using Alphafold[75].

553 **Plasmid construction**

554 Luciferase constructs for the luminescence-based SCR assay were generated in the
555 reconstructive pFN19K T7 SP6 flexi vector (Promega Corporation). The coding
556 sequences of the tested genes, *ZmH3C2*, *ZmCEQORH*, *ZmBTF3* and
557 *Zm00001d009138*, along with their canonical stop codons and inter-stop codon
558 regions (ISRs, the extension regions) were cloned upstream of the coding sequence of
559 the firefly luciferase gene (*Fluc*) without ATG between *EcoRI* and *KpnI* sites. A linker
560 sequence (5′ GGCGGCTCCGGCGGCTCCCTCGTGCTCGGG 3′) was added

561 upstream of the Fluc sequence to avoid potential distortions between the tested protein
562 and Fluc in the fusion protein[15,31,38]. Primer sequences are listed in Supplementary
563 Table 15.

564 For subcellular localization analysis, the ZmBTF3 and ZmBTF3x coding
565 sequences were introduced into the pAN580 vector containing the 35S promoter and
566 the coding sequence for GFP. GFP was fused to the C-terminus of ZmBTF3 and
567 ZmBTF3x. Primer sequences are listed in Supplementary Table 15.

568 ***In vitro* translation for SCR Assay**

569 For SCR assay, we used *in vitro* translation system based on Wheat Germ Extract
570 (Promega Corporation), which has been used for SCR validation as reported
571 previously[31,38]. The constructed plasmid DNA including the test gene and *Fluc* (no
572 ATG) was linearized using BamH I or XbaI enzyme, and 2 μg of the linearized DNA
573 was transcribed *in vitro* using T7 RNA polymerase (Promega Corporation). The
574 obtained RNA was then purified using GeneJET kit (Thermo Fisher Scientific). The
575 concentration and purity of the RNA were measured using Nanodrop 2000 (Thermo
576 Fisher Scientific). A total of 2 μg purified RNA was translated *in vitro* using the
577 Wheat Germ Extract at 25 °C for 2 h according to the manufacturer′s instructions.
578 Luciferase activity was then measured at room temperature (below 25 °C) using the
579 Luciferase Assay System (Promega Corporation) in a Glomax luminometer (Promega
580 Corporation) with a 10-s measurement read for luciferase activity.

581 **Immunoblotting and mass spectrometric analysis**

582 The proteins extracted from the *in vitro* protein expression system were separated by
583 10% (w/v) SDS-polyacrylamide gel electrophoresis (SDS-PAGE). One PAGE gel was
584 stained with Coomassie Brilliant Blue (CBB), while another was transferred to a
585 polyvinylidene difluoride membrane (0.22 μm, Millipore). Proteins were detected by
586 immunoblotting with anti-Fluc antibodies (1:10,000, ab185924, Abcam). The regions
587 of interest in the CBB staining gel were excised manually according to the
588 immunoblotting band, and then destained with 30% (v/v) ACN in 100 mM NH_4HCO_3
589 and dried in a vacuum centrifuge. The extracted proteins were reduced with

590 dithiothreitol (DTT) (10 mM DTT in 100 mM NH_4HCO_3) for 30 min at 56 °C, then
591 alkylated with iodoacetamide (200 mM IAA in 100 mM NH_4HCO_3) in the dark at
592 room temperature for 30 min. Gel pieces were briefly rinsed with 100 mM NH_4HCO_3
593 and ACN, respectively. The gel pieces were then divided equally into three parts and
594 separately digested overnight in 12.5 ng/μl trypsin, overnight in chymotrypsin in 25
595 mM NH_4HCO_3, and for 30 min in 12.5 ng/μl pepsin in PH3 HCl. The peptides were
596 extracted using 60% (v/v) ACN in 0.1% (v/v) trifluoroacetic acid (TFA) three times,
597 and the extracts were pooled and dried completely by a vacuum centrifuge.

598 LC-MS/MS was performed on a Q-Exactive HF-X mass spectrometer coupled to
599 Easy nLC 1200 (Thermo Fisher Scientific). The peptide mixture was loaded onto a
600 C18-reversed phase column (15 cm, 75 μm inner diameter) packed in-house with RP-
601 C18 (5 μm resin, Thermo Fisher Scientific) in buffer A (0.1% [v/v] formic acid in
602 HPLC-grade water) and separated with a linear gradient of buffer B (0.1% formic acid
603 in 84% [v/v] ACN) at a flow rate of 250 nl/min controlled by IntelliFlow technology
604 over 60 min. MS data were acquired using a data-dependent top-10 method
605 dynamically choosing the most abundant precursor ions from the survey scan (m/z
606 300-1,800) for HCD fragmentation. The target value was determined based on pAGC.
607 The dynamic exclusion duration was 20 s. Survey scans were acquired at a resolution
608 of 70,000 (m/z 200) and the resolution for HCD spectra was set to 17,500 (m/z 200).
609 Normalized collision energy was 27 eV and the underfill ratio, which specifies the
610 minimum percentage of the target value likely to be reached at maximum fill time,
611 was defined as 0.1%.

612 The MS data were then separately searched against the target protein sequences
613 (readthrough protein sequences of *H3C2*, *ZmCEQORH*, and *ZmBTF3*) using
614 MaxQuant software (v.1.6.1.10)[61]. An initial search was set with a precursor mass
615 window of 6 ppm. The search followed an enzymatic cleavage rule of "unspecified"
616 and a mass tolerance of 20 ppm for fragment ions. Carbamidomethylation of cysteines
617 was defined as fixed modification, while methionine oxidation was defined as
618 variable modification for database searching. The cutoff of the global FDR for peptide

619 and protein identification was set to 0.01.

620 **Subcellular localization of ZmBTF3-GFP and ZmBTF3x-GFP fusions.**

621 The GFP fusion plasmids were transformed into maize mesophyll protoplasts by
622 polyethylene glycol-mediated transformation. Protoplast preparation and transfection
623 were conducted as previously described[76]. A plasma membrane-localized marker
624 *35S:ZmPDCK7-mCherry* and a nucleus-localized marker *35S:AtHY5-mCherry* were
625 used for colocalization analyses[77,78]. Fluorescence signals were observed on a
626 confocal laser scanning microscope (LSM800, Zeiss).

627 ## Data availability

628 All data generated or analyzed in this study are included in this article or the
629 Supplementary Information and Tables. The raw datasets of proteomics have been
630 deposited at the ProteomeXchange under the accession ID PXD035958 and
631 PXD038762. Source data are provided.

632 ## Code availability

633 Custom codes are available for research purposes from the corresponding authors
634 upon request.

635 **References**

636 1. Baranov, P. V., Atkins, J. F. & Yordanova, M. M. Augmented genetic decoding:
637 global, local and temporal alterations of decoding processes and codon
638 meaning. *Nat. Rev. Genet.* **16**, 517-529 (2015).
639 2. Freitag, J., Ast, J. & Bolker, M. Cryptic peroxisomal targeting via alternative
640 splicing and stop codon read-through in fungi. *Nature* **485**, 522-525 (2012).
641 3. Bazykin, G. A. & Kochetov, A. V. Alternative translation start sites are
642 conserved in eukaryotic genomes. *Nucleic Acids Res.* **39**, 567-577 (2011).
643 4. Jacks, T. & Varmus, H. E. Expression of the Rous sarcoma virus *pol* gene by
644 ribosomal frameshifting. *Science* **230**, 1237-1242 (1985).
645 5. Lang, B. F. et al. Massive programmed translational jumping in mitochondria.
646 *Proc. Natl Acad. Sci. USA* **111**, 5926-5931 (2014).
647 6. Sapkota, D. et al. Cell-type-specific profiling of alternative translation
648 Identifies regulated protein isoform variation in the mouse brain. *Cell Rep.* **26**,
649 594-607.e597 (2019).
650 7. Rodnina, M. V. et al. Translational recoding: canonical translation mechanisms
651 reinterpreted. *Nucleic Acids Res.* **48**, 1056-1067 (2020).
652 8. Palma, M. & Lejeune, F. Deciphering the molecular mechanism of stop codon
653 readthrough. *Biol. Rev. Camb. Philos. Soc.* **96**, 310-329 (2021).
654 9. Torabi, N. & Kruglyak, L. Genetic basis of hidden phenotypic variation
655 revealed by increased translational readthrough in yeast. *PLoS Genet.* **8**,
656 e1002546 (2012).
657 10. Namy, O., Duchateau-Nguyen, G. & Rousset, J. P. Translational readthrough
658 of the *PDE2* stop codon modulates cAMP levels in *Saccharomyces cerevisiae*.
659 *Mol. Microbiol.* **43**, 641-652 (2002).
660 11. Dunn, J. G., Foo, C. K., Belletier, N. G., Gavis, E. R. & Weissman, J. S.
661 Ribosome profiling reveals pervasive and regulated stop codon readthrough in
662 *Drosophila melanogaster*. *eLife* **2**, e01179 (2013).
663 12. Xue, F. & Cooley, L. *kelch* encodes a component of intercellular bridges in

664 *Drosophila* egg chambers. *Cell* **72**, 681-693 (1993).
665 13. Karki, P. et al. Tissue-specific regulation of translational readthrough tunes
666 functions of the traffic jam transcription factor. *Nucleic Acids Res.* (2021).
667 14. Schueren, F. et al. Peroxisomal lactate dehydrogenase is generated by
668 translational readthrough in mammals. *eLife* **3**, e03640 (2014).
669 15. Eswarappa, S. M. et al. Programmed translational readthrough generates
670 antiangiogenic VEGF-Ax. *Cell* **157**, 1605-1618 (2014).
671 16. Xin, H., Zhong, C., Nudleman, E. & Ferrara, N. Evidence for pro-angiogenic
672 functions of VEGF-Ax. *Cell* **167**, 275-284.e276 (2016).
673 17. Weiner, A. M. & Weber, K. Natural read-through at the UGA termination
674 signal of Q-beta coat protein cistron. *Nat. New Biol.* **234**, 206-209 (1971).
675 18. Pelham, H. R. Leaky UAG termination codon in tobacco mosaic virus RNA.
676 *Nature* **272**, 469-471 (1978).
677 19. Yoshinaka, Y., Katoh, I., Copeland, T. D. & Oroszlan, S. Murine leukemia
678 virus protease is encoded by the *gag-pol* gene and is synthesized through
679 suppression of an amber termination codon. *Proc. Natl Acad. Sci. USA* **82**,
680 1618-1622 (1985).
681 20. True, H. L. & Lindquist, S. L. A yeast prion provides a mechanism for genetic
682 variation and phenotypic diversity. *Nature* **407**, 477-483 (2000).
683 21. Namy, O. et al. Identification of stop codon readthrough genes in
684 *Saccharomyces cerevisiae*. *Nucleic Acids Res.* **31**, 2289-2296 (2003).
685 22. Baudin-Baillieu, A. et al. Genome-wide translational changes induced by the
686 prion [PSI+]. *Cell Rep.* **8**, 439-448 (2014).
687 23. Jungreis, I. et al. Evidence of abundant stop codon readthrough in *Drosophila*
688 and other metazoa. *Genome Res.* **21**, 2096-2113 (2011).
689 24. Jungreis, I. et al. Evolutionary dynamics of abundant stop codon readthrough.
690 *Mol. Biol. Evol.* **33**, 3108-3132 (2016).
691 25. Hudson, A. M. et al. Tissue-specific dynamic codon redefinition in *Drosophila*.
692 *Proc. Natl Acad. Sci. USA* **118** (2021).

693 26. Klagges, B. R. et al. Invertebrate synapsins: a single gene codes for several
694 isoforms in Drosophila. *J Neurosci.* **16**, 3154-3165 (1996).
695 27. Steneberg, P. & Samakovlis, C. A novel stop codon readthrough mechanism
696 produces functional Headcase protein in *Drosophila* trachea. *EMBO Rep* 2,
697 593-597 (2001).
698 28. Geller, A. I. & Rich, A. A UGA termination suppression tRNATrp active in
699 rabbit reticulocytes. *Nature* **283**, 41-46 (1980).
700 29. Yamaguchi, Y. et al. L-MPZ, a novel isoform of myelin P0, is produced by
701 stop codon readthrough. *J. Biol. Chem.* **287**, 17765-17776 (2012).
702 30. Manjunath, L. E. et al. Stop codon read-through of mammalian *MTCH2*
703 leading to an unstable isoform regulates mitochondrial membrane potential. *J.*
704 *Biol. Chem.* **295**, 17009-17026 (2020).
705 31. Singh, A. et al. Let-7a-regulated translational readthrough of mammalian
706 *AGO1* generates a microRNA pathway inhibitor. *EMBO J.* **38**, e100727 (2019).
707 32. Loughran, G. et al. Evidence of efficient stop codon readthrough in four
708 mammalian genes. *Nucleic Acids Res.* **42**, 8928-8938 (2014).
709 33. De Bellis, M. et al. Translational readthrough generates new astrocyte AQP4
710 isoforms that modulate supramolecular clustering, glial endfeet localization,
711 and water transport. *Glia* **65**, 790-803 (2017).
712 34. Stiebler, A. C. et al. Ribosomal readthrough at a short UGA stop codon context
713 triggers dual localization of metabolic enzymes in Fungi and animals. *PLoS*
714 *Genet.* **10**, e1004685 (2014).
715 35. Loughran, G. et al. Stop codon readthrough generates a C-terminally extended
716 variant of the human vitamin D receptor with reduced calcitriol response. *J.*
717 *Biol. Chem.* **293**, 4434-4444 (2018).
718 36. Yordanova, M. M. et al. *AMD1* mRNA employs ribosome stalling as a
719 mechanism for molecular memory formation. *Nature* **553**, 356-360 (2018).
720 37. Yordanova, M. M., Loughran, G., Atkins, J. F. & Baranov, P. V. Stop codon
721 readthrough contexts influence reporter expression differentially depending on

722 the presence of an IRES. *Wellcome Open Res.* **5**, 221 (2020).
723 38. Sahoo, S. et al. Identification and functional characterization of mRNAs that
724 exhibit stop codon readthrough in *Arabidopsis thaliana*. *J. Biol. Chem.* **298**,
725 102173 (2022).
726 39. Blanchet, S., Cornu, D., Argentini, M. & Namy, O. New insights into the
727 incorporation of natural suppressor tRNAs at stop codons in *Saccharomyces*
728 *cerevisiae*. *Nucleic Acids Res.* **42**, 10061-10072 (2014).
729 40. Feng, Y. X., Copeland, T. D., Oroszlan, S., Rein, A. & Levin, J. G.
730 Identification of amino acids inserted during suppression of UAA and UGA
731 termination codons at the *gag-pol* junction of Moloney murine leukemia virus.
732 *Proc. Natl Acad. Sci. USA* **87**, 8860-8863 (1990).
733 41. Roy, B., Leszyk, J. D., Mangus, D. A. & Jacobson, A. Nonsense suppression
734 by near-cognate tRNAs employs alternative base pairing at codon positions 1
735 and 3. *Proc. Natl Acad. Sci. USA* **112**, 3038-3043 (2015).
736 42. Strigini, P. & Brickman, E. Analysis of specific misreading in *Escherichia coli*.
737 *J. Mol. Biol.* **75**, 659-672 (1973).
738 43. Sánchez-Silva, R., Villalobo, E., Morin, L. & Torres, A. A new noncanonical
739 nuclear genetic code: translation of UAA into glutamate. *Curr. Biol.* **13**, 442-
740 447 (2003).
741 44. Blanchet, S. et al. Deciphering the reading of the genetic code by near-cognate
742 tRNA. *Proc. Natl Acad. Sci. USA* **115**, 3018-3023 (2018).
743 45. Choi, S. et al. Proteogenomic Approach to UTR Peptide Identification. *J*
744 *Proteome Res.* **19**, 212-220 (2019).
745 46. Aerni, H. R., Shifman, M. A., Rogulina, S., O'Donoghue, P. & Rinehart, J.
746 Revealing the amino acid composition of proteins within an expanded genetic
747 code. *Nucleic Acids Res.* **43**, e8 (2015).
748 47. Valle, R. P., Morch, M. D. & Haenni, A. L. Novel amber suppressor tRNAs of
749 mammalian origin. *EMBO J.* **6**, 3049-3055 (1987).
750 48. Namy, O., Hatin, I. & Rousset, J. P. Impact of the six nucleotides downstream

751 of the stop codon on translation termination. *EMBO Rep.* **2**, 787-793 (2001).
752 49. Tork, S., Hatin, I., Rousset, J. P. & Fabret, C. The major 5' determinant in stop
753 codon read-through involves two adjacent adenines. *Nucleic Acids Res.* **32**,
754 415-421 (2004).
755 50. Mangkalaphiban, K. et al. Transcriptome-wide investigation of stop codon
756 readthrough in *Saccharomyces cerevisiae*. *PLoS Genet.* **17**, e1009538 (2021).
757 51. Chan, P. P., Lin, B. Y., Mak, A. J. & Lowe, T. M. tRNAscan-SE 2.0: improved
758 detection and functional classification of transfer RNA genes. *Nucleic Acids*
759 *Res.* **49**, 9077-9096 (2021).
760 52. Laslett, D. & Canback, B. ARAGORN, a program to detect tRNA genes and
761 tmRNA genes in nucleotide sequences. *Nucleic Acids Res.* **32**, 11-16 (2004).
762 53. Ding, Y. et al. OST1-mediated BTF3L phosphorylation positively regulates
763 CBFs during plant cold responses. *EMBO J.* **37**, *e98228* (2018).
764 54. Atkins, J. F. & Baranov, P. V. The distinction between recoding and codon
765 reassignment. *Genetics* **185**, 1535-1536 (2010).
766 55. Ivanova, N. N. et al. Stop codon reassignments in the wild. *Science* **344**, 909-
767 913 (2014).
768 56. Swart, E. C., Serra, V., Petroni, G. & Nowacki, M. Genetic codes with no
769 dedicated stop codon: context-dependent translation termination. *Cell* **166**,
770 691-702 (2016).
771 57. Beier, H. & Grimm, M. Misreading of termination codons in eukaryotes by
772 natural nonsense suppressor tRNAs. *Nucleic Acids Res.* **29**, 4767-4782 (2001).
773 58. Dabrowski, M., Bukowy-Bieryllo, Z. & Zietkiewicz, E. Translational
774 readthrough potential of natural termination codons in eucaryotes--The impact
775 of RNA sequence. *RNA Biol.* **12**, 950-958 (2015).
776 59. Schimmel, P. The emerging complexity of the tRNA world: mammalian tRNAs
777 beyond protein synthesis. *Nat. Rev. Mol. Cell Biol.* **19**, 45-58 (2018).
778 60. Wiśniewski, J. R., Zougman, A., Nagaraj, N. & Mann, M. Universal sample
779 preparation method for proteome analysis. *Nat. Methods* **6**, 359-362 (2009).

780 61. Tyanova, S., Temu, T. & Cox, J. The MaxQuant computational platform for
781 mass spectrometry-based shotgun proteomics. *Nat. Protoc.* **11**, 2301-2319
782 (2016).
783 62. Lei, L. et al. Ribosome profiling reveals dynamic translational landscape in
784 maize seedlings under drought stress. *Plant J.* **84**, 1206-1218 (2015).
785 63. Chotewutmontri, P. & Barkan, A. Dynamics of chloroplast translation during
786 chloroplast differentiation in maize. *PLoS Genet.* **12**, e1006106 (2016).
787 64. Chotewutmontri, P. & Barkan, A. Multilevel effects of light on ribosome
788 dynamics in chloroplasts program genome-wide and psbA-specific changes in
789 translation. *PLoS Genet.* **14**, e1007555 (2018).
790 65. Zoschke, R., Chotewutmontri, P. & Barkan, A. Translation and co-translational
791 membrane engagement of plastid-encoded chlorophyll-binding proteins are
792 not influenced by chlorophyll availability in maize. *Front. Plant. Sci.* **8**, 385
793 (2017).
794 66. Jiang, J. et al. An RNA chaperone-like protein plays critical roles in
795 chloroplast mRNA stability and translation in *Arabidopsis* and maize. *Plant*
796 *Cell* **31**, 1308-1327 (2019).
797 67. Dobin, A. et al. STAR: ultrafast universal RNA-seq aligner. *Bioinformatics* **29**,
798 15-21 (2013).
799 68. Machanick, P. & Bailey, T. L. MEME-ChIP: motif analysis of large DNA
800 datasets. *Bioinformatics* **27**, 1696-1697 (2011).
801 69. Gupta, S., Stamatoyannopoulos, J. A., Bailey, T. L. & Noble, W. S.
802 Quantifying similarity between motifs. *Genome Biol.* **8**, R24 (2007).
803 70. Lorenz, R. et al. ViennaRNA Package 2.0. *Algorithms Mol. Biol.* **6**, 26 (2011).
804 71. Krogh, A., Larsson, B., von Heijne, G. & Sonnhammer, E. L. Predicting
805 transmembrane protein topology with a hidden Markov model: application to
806 complete genomes. *J. Mol. Biol.* **305**, 567-580 (2001).
807 72. Kosugi, S., Hasebe, M., Tomita, M. & Yanagawa, H. Systematic identification
808 of cell cycle-dependent yeast nucleocytoplasmic shuttling proteins by

809 prediction of composite motifs. *Proc. Natl Acad. Sci. USA* **106**, 10171-10176
810 (2009).
811 73. Neuberger, G., Maurer-Stroh, S., Eisenhaber, B., Hartig, A. & Eisenhaber, F.
812 Prediction of peroxisomal targeting signal 1 containing proteins from amino
813 acid sequence. *J. Mol. Biol.* **328**, 581-592 (2003).
814 74. Maurer-Stroh, S. & Eisenhaber, F. Refinement and prediction of protein
815 prenylation motifs. *Genome Biol.* **6**, R55 (2005).
816 75. Jumper, J. et al. Highly accurate protein structure prediction with AlphaFold.
817 *Nature* **596**, 583-589 (2021).
818 76. Yoo, S. D., Cho, Y. H. & Sheen, J. *Arabidopsis* mesophyll protoplasts: a
819 versatile cell system for transient gene expression analysis. *Nat. Protoc.* **2**,
820 1565-1572 (2007).
821 77. Zhao, Y. et al. The calcium-dependent protein kinase ZmCDPK7 functions in
822 heat-stress tolerance in maize. *J. Integr. Plant. Biol.* **63**, 510-527 (2021).
823 78. Li, Y. et al. Plasma membrane-nucleo-cytoplasmic coordination of a receptor-
824 like cytoplasmic kinase promotes EDS1-dependent plant immunity. *Nat.*
825 *Plants* **8**, 802-816 (2022).

Acknowledgments

This study was supported by the National Natural Science Foundation of China (no. 32172073, U22A20474, 31872872), the National Key Research and Development Program of China (2022YFD1201802), and the Seed-Industrialized Development Program in Shandong Province (no. 2021LZGC003). We are grateful to Steven P. Briggs and David Backhouse for their constructive comments and suggestions. We also thank Dr. Anguo Sun and Dr. Yanwen Xiang for the technical assistance and Yingying Sha and Mengxia Niu for their assistance with the microscopic observations.

Author Contributions

L.W., S.-B.W., and Z.T. designed the project. Y. Zhang, Y.S., L.T., H.Y., A.X., J.Z., U.A., A.S., X.C. and Y.C. were involved in bioinformatics analysis. Y. Zhang, H.L., S.W. and J.S. conducted the experiments. C.G., Y. Zhao, Y. L. and X.W. collected the materials for mass spectrometry detection and subsequent experiments. Y. Zhang, H.L. and Y.S. wrote the manuscript. L.W., S.-B.W., and Z.T. contributed substantially to revisions. All authors read and approved the manuscript.

Competing interests

The authors declare no competing interests.

845 # Figures

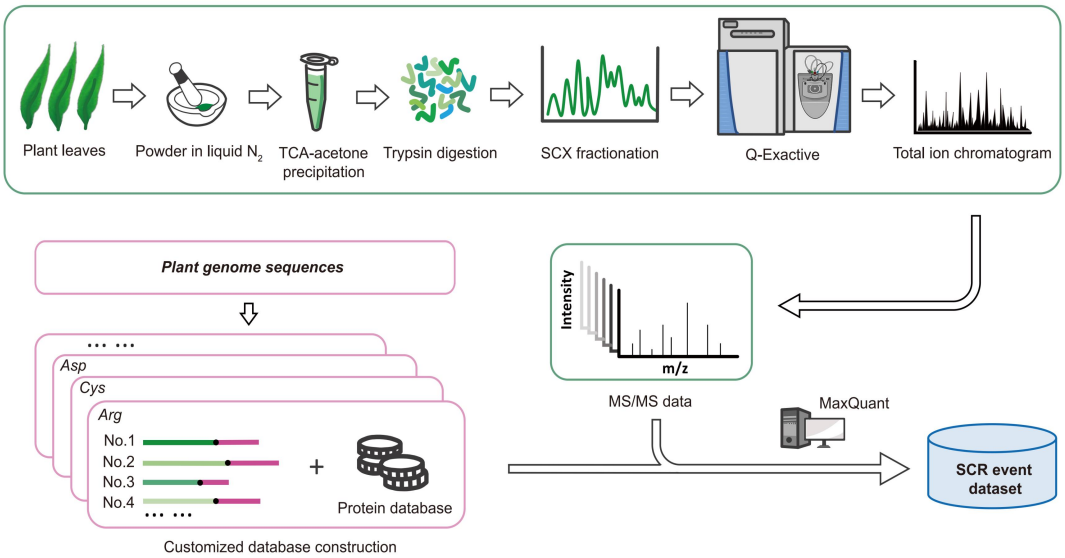

846 **Fig. 1 | Proteogenomic workflow for identifying plant stop codon readthrough (SCR)**
847 **events.** The strategy consists of two procedures: shotgun proteomics experiment (green box)
848 and customized database construction (pink boxes). Total protein was extracted from plant
849 leaves and subjected to digestion, fragmentation, and LC-MS/MS analysis for identification
850 of spectra datasets. Customized databases were constructed as described in Methods. MS/MS
851 spectra datasets were searched against the 20 customized databases merged with the public
852 plant protein database by the MaxQuant. We defined the MS/MS-identified peptides that
853 exclusively spanned the annotated stop codon sites as "through" peptides, and classified
854 proteins sharing a unique stop codon site and containing a "through" peptide as one SCR
855 event.

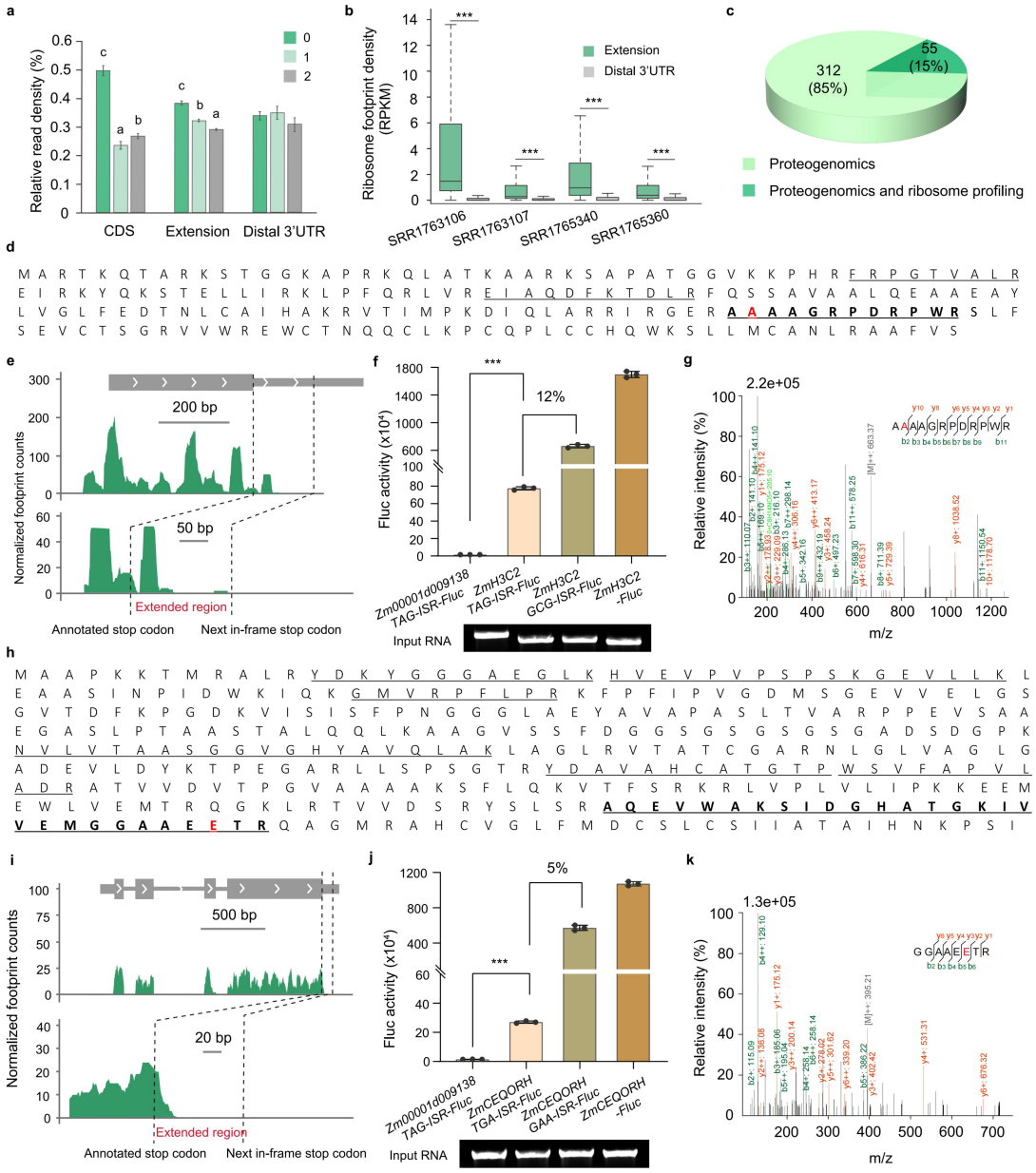

Fig. 2 | Verifying SCR events in maize. a Three-nucleotide periodicity of 30-mers in the CDSs, putative extensions, and the distal 3′ UTRs. Data are mean ± s.d. Different letters indicate significant differences at $P < 0.05$ by one-way ANOVA with Tukey's multiple comparisons test. Green, light green, and gray bars represent frame 0, 1, and 2, respectively. **b** Distribution of ribosome footprint density in putative extensions and the distal 3′ UTRs in the four Ribo-seq datasets. Distal 3′ UTR was defined as the region 40 codons after the next stop-codon or the region from the next stop-codon to the third stop codon within 40 codons. Box edges represent the 0.25 and 0.75 quantiles. The bold lines represent the median and whiskers represent 1.5×IQR. Statistical significance was determined using a two-sided Student's *t*-test,

865 ***$P < 0.001$. **c** The proportion of SCR events confirmed by ribosome profiling among those
866 identified by proteogenomics. **d-k** Validation of two readthrough examples, *ZmH3C2* (**d-g**)
867 and *ZmCEQORH* (**h-k**). **d, h** The complete protein sequences extended to the next in-frame
868 stop codon of the two genes showing the underlined peptides identified by mass spectrometry
869 analysis, and the readthrough peptides are in bold. The amino acids translated at the stop
870 codon sites in readthrough peptides are highlighted in red, which are alanine (A) at UAG (**d**)
871 and glutamate (E) at UGA (**h**). **e, i** Ribo-seq analysis revealing clear footprint signals in the C-
872 terminal extensions of the two transcripts. Dashed lines represent the annotated stop codon
873 and the next in-frame stop codon. **f, j** *In vitro* translation experiment showing readthrough
874 activities of *ZmH3C2* and *ZmCEQORH*. Plasmids containing test cDNA-stop codon-ISR-*Fluc*
875 were firstly transcribed *in vitro*, followed by *in vitro* translation using wheat germ extract.
876 Luciferase activities were used to represent the readthrough activities. Constructs with the
877 stop codon mutated to a sense codon were used as a positive control of the translation to
878 measure the efficiency of SCR. The non-SCR gene *Zm00001d009138* with its TAG and ISR
879 sequence fused with *Fluc* (*Zm00001d009138-TAG-ISR-Fluc*) was used as the SCR-negative
880 control, as it showed no SCR sign in either proteogenomics or Ribo-seq analysis. All samples
881 were tested in biological triplicates. Data are mean ± s.e.m (n=3). Asterisks indicate statistical
882 significance by two-sided Student's *t*-test (***$P < 0.001$). ISR, inter-stop codon region
883 (extension region). **g, k** MS/MS spectra of the identified readthrough peptides
884 AAAAGRPDRPWR for *ZmH3C2* (**g**) and GGAAEETR for *ZmCEQORH* **(k)** readthrough
885 products expressed from (**f**) and (**j**), respectively. Source data are provided as a Source Data
886 file.

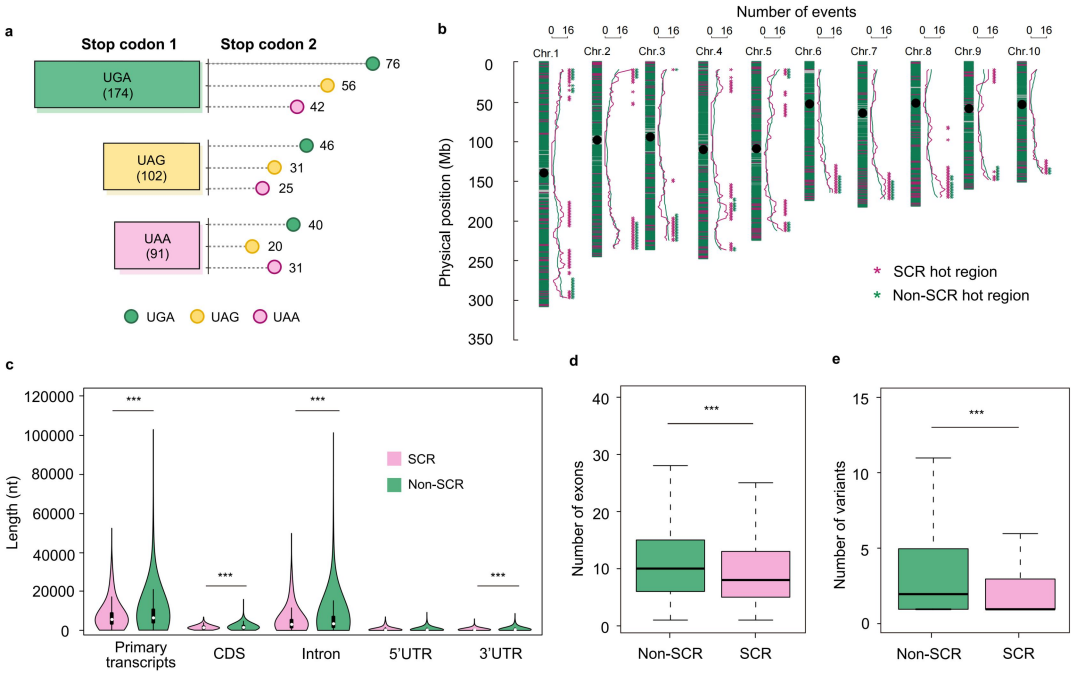

Fig. 3 | Characteristics of SCR events in maize. a Stop codon usage and the next stop codon preference in SCR events. Stop codon 1, readthrough stop codon; Stop codon 2, the next in-frame stop codon. **b** Genome-wide distribution of SCR (pink) and non-SCR (green) events in maize. For each chromosome, the distribution contains three columns. Left: SCR (pink) and non-SCR (green) events across the chromosomes. Black dots are centromeres. Middle: distribution patterns of SCR (pink) and non-SCR (green) events are shown by curves, shown as a 20-Mb sliding window with a 2-Mb step based on the B73 reference genome. Right: distribution of hotspot regions for SCR (pink) and non-SCR (green) events shown with asterisks. We defined hotspot regions as ≥5 SCR events and ≥335 non-SCR events in a 20-Mb window. **c** Violin plot describing the length distribution of primary transcripts and transcript elements in SCR and non-SCR events. The length of the primary transcript is the sum of CDSs, introns, and UTRs. CDS length represents the length of the open reading frame (ORF). Internal boxplots show the median values (white dots in the center) and the interquartile range (IQR; 0.25 and 0.75 quantiles) of the length distribution. **d** Number of exons in SCR and non-SCR primary transcripts. **e** Number of splice variants in SCR and non-SCR primary transcripts. For all boxplots, box edges represent the 0.25 and 0.75 quantiles. The bold lines represent the median values and the whiskers represent 1.5×IQR. ***$P < 0.001$ (two-sided Student's *t*-test). Source data are provided as a Source Data file.

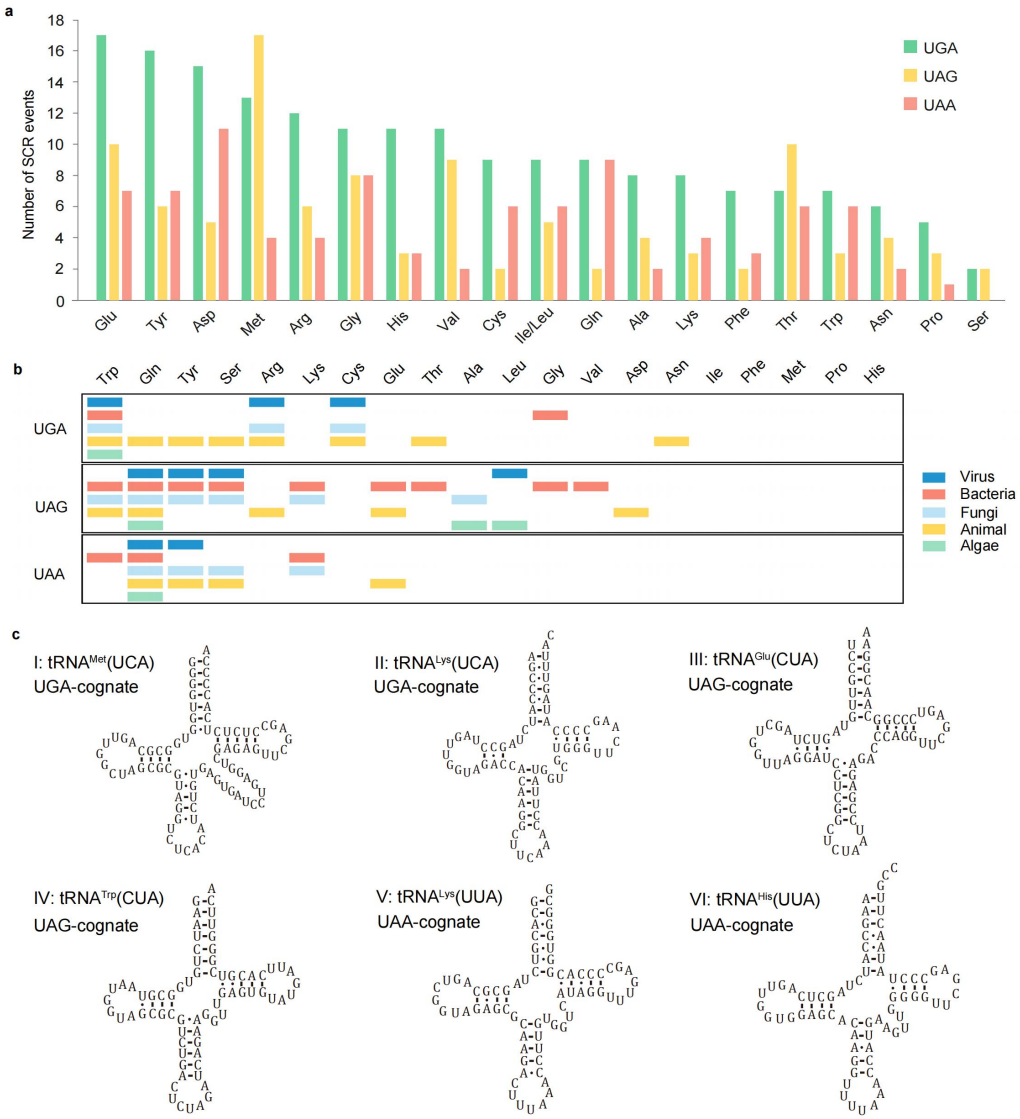

Fig. 4 | Stop codons are recoded as 20 amino acids in maize SCR events. a Frequency of amino acids specified by the three stop codons. The x-axis represents the 20 standard amino acids. The y-axis is the number of SCR events. **b** Previously reported amino acids translated at UGA, UAG, and UAA in different species. Blue, virus; orange, bacteria; light blue, fungi; yellow, animal; green, algae. **c** Examples of UGA-, UAG-, and UAA suppressor tRNAs identified by tRNAscan-SE and ARAGORN corresponding to amino acids shown at UGA, UAG, and UAA. The predicted secondary structures of the tRNAs are shown (I-VI): $tRNA^{Met}$ (UCA) and $tRNA^{Lys}$ (UCA) recognize UGA, $tRNA^{Glu}$ (CUA) and $tRNA^{Trp}$ (CUA) recognize UAG, and $tRNA^{Lys}$ (UUA) and $tRNA^{His}$ (UUA) recognize UAA.

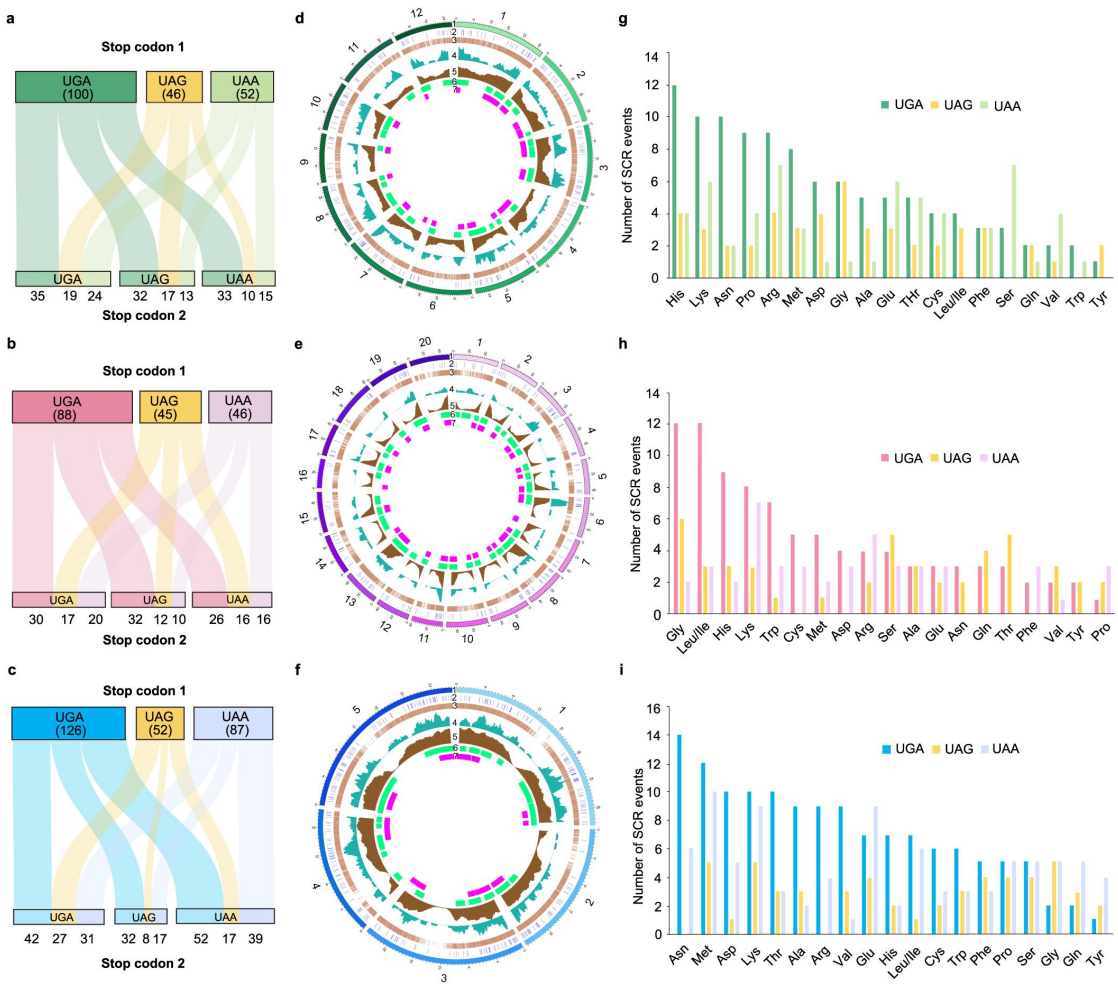

Fig. 5 | SCR events and recoding plasticity of stop codons in other plants. a, b, c Stop codon usage and the next stop codon preference of SCR events in rice (**a**), soybean (**b**), and *Arabidopsis* (**c**). Stop codon 1, readthrough stop codon; Stop codon 2, the next in-frame stop codon. **d, e, f** Circos plots showing the genome-wide distribution of SCR and non-SCR events in rice (**d**), soybean (**e**), and *Arabidopsis* (**f**). Each Circos plot consists of seven layers. 1, chromosomes; 2-3, distribution patterns of SCR (2) and non-SCR (3) events across the chromosomes; 4-5, distribution patterns of SCR (4) and non-SCR (5) events determined using a window size of 4 Mb with a step of 400 kb based on the Nipponbare reference genome for rice, a 10-Mb window with a 1-Mb step based on the ZH13 reference genome, and a 1.2-Mb window with a 100-kb step based on the Columbia-0 reference genome; 6-7, distribution of hotspot regions for SCR (6) and non-SCR (7) events. Hotspot regions were defined as ≥3 SCR events and ≥178 non-SCR events in a 4-Mb window for rice, ≥2 SCR events and ≥253 non-SCR events in a 10-Mb window for soybean, and ≥4 SCR events and ≥157 for non-SCR events in a 1.2-Mb window for *Arabidopsis*. **g, h, i** Frequency of amino acids specified by the

928 three stop codons in rice (**g**), soybean (**h**), and *Arabidopsis* (**i**) SCR events. The x-axis
929 represents the 20 standard amino acids. The y-axis is the number of SCR events.

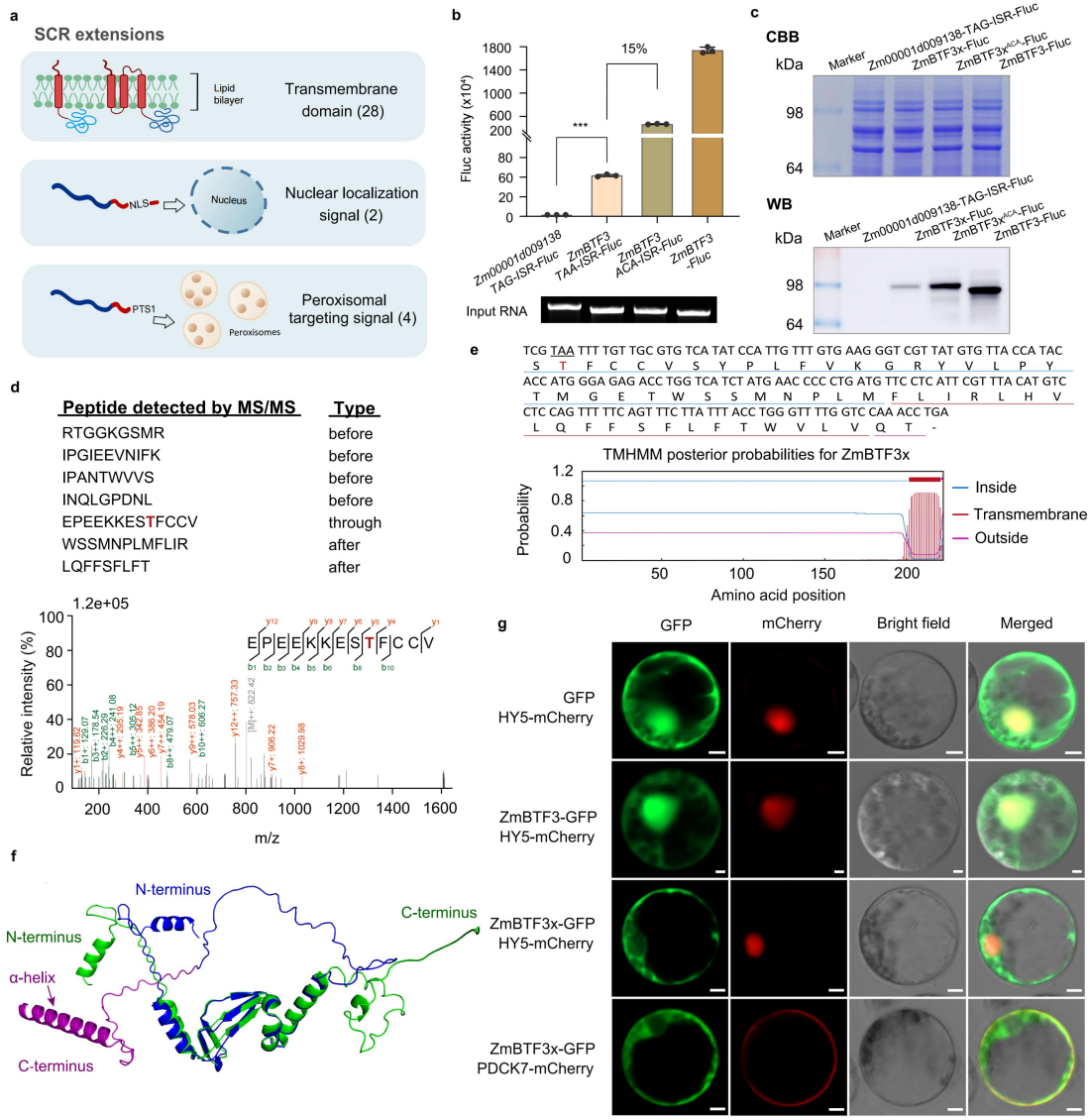

Fig. 6 | C-terminal extensions in maize SCR events contain multiple functional signals. a Multiple functional signals predicted in the extensions of SCR events. **b** Readthrough validation of *ZmBTF3* using the *in vitro* translation experiment. The plasmid containing *ZmBTF3-TAA-ISR-Fluc* was firstly transcribed *in vitro*, followed by *in vitro* translation using wheat germ extract. *ZmBTF3* with TAA mutated to ACA was used as the positive control of the translation to measure the efficiency of SCR. The *Zm00001d009138-TAG-ISR-Fluc* was used as the SCR-negative control. Luciferase activity reflects the readthrough activity. All experiments were performed in triplicates. Data are mean ± s.e.m (n=3). Statistical difference was calculated using a two-sided Student's *t*-test, ***$P < 0.001$. ISR, inter-stop codon region. **c** SDS-PAGE and immunoblot analysis of the ZmBTF3x-Fluc (ZmBTF3-TAA-ISR-Fluc), ZmBTF3x^{ACA}-Fluc (ZmBTF3-ACA-ISR-Fluc), and ZmBTF3-Fluc fusion proteins. Top:

941 Coomassie Brilliant Blue (CBB)-stained gel of the expressed products derived from (**b**).
942 Bottom: Immunoblot of the ZmBTF3x-Fluc, ZmBTF3x^{ACA}-Fluc, and ZmBTF3-Fluc fusion
943 proteins using an anti-Fluc antibody. The ZmBTF3x^{ACA}-Fluc was used as the positive control.
944 The Zm00001d009138-TAG-ISR-Fluc was used as the negative control. ISR, inter-stop codon
945 region. **d** MS/MS analysis of the digested peptides of the ZmBTF3x-Fluc fusion protein
946 excised from the CBB gel in (**c**). The sequences of MS-detected peptides, labeled as "before",
947 "through", and "after", are shown on the top. An MS/MS spectrum of the "through" peptide
948 EPEEKKESTFCCV is shown on the bottom. UAA was recoded as threonine (T) shown in red.
949 **e** Transmembrane domain prediction in the C-terminus of ZmBTF3x using the TMHMM
950 server. The blue, red, and magenta lines represent residues 1-201 inside the membrane, 202-
951 221 as a transmembrane helix, and 222-223 outside the membrane, respectively. The amino
952 acid sequence from the annotated stop codon to the next stop codon of BTF3x is shown on the
953 top. **f** AlphaFold structural models for ZmBTF3 and its readthrough protein ZmBTF3x. Green:
954 ZmBTF3; dark blue: parent protein region of the readthrough protein ZmBTF3x; magenta: C-
955 terminal extension region of ZmBTF3x. The predicted α-helix is shown at the C-terminus. **g**
956 Subcellular localization of ZmBTF3 and ZmBTF3x. Constructs encoding C-terminal GFP
957 fusions of ZmBTF3 or ZmBTF3x were transfected into maize protoplasts for localization
958 assays under a confocal microscope. GFP-vector transfected protoplasts were used as the
959 control. The experiments were performed three times with similar results. HY5-mCherry was
960 the nucleus marker and PDCK7-mCherry was the plasma membrane marker. Scale bars, 5 μm.
961 Source data are provided as a Source Data file.

962 **Supplementary Information, Tables and Dataset have been submitted**
963 **as separate files.**
964
965 **Supplementary Information contains Supplementary Figures 1-10 and**
966 **References for Supplementary Table 5**
967
968 **Supplementary Table 1. SCR events identified in maize by proteogenomics.**
969 **Supplementary Table 2. Peptides identified by mass spectrometry for SCR and**
970 **parent proteins in maize.**
971 **Supplementary Table 3. SCR events detected in maize by both proteogenomics**
972 **and ribosome profiling.**
973 **Supplementary Table 4. Non-SCR events identified in maize by proteogenomics.**
974 **Supplementary Table 5. Standard amino acids translated by stop codons in the**
975 **literature and their translation evidence in maize. I, UGA; II, UAG; III, UAA.**
976 **UGA-, UAG-, and UAA suppressor tRNAs were predicted by tRNAscan-SE or**
977 **ARAGORN.**
978 **Supplementary Table 6. Predicted suppressor tRNAs in maize aligned with**
979 **tRNAs in the NCBI NT database.**
980 **Supplementary Table 7. SCR events identified in rice by proteogenomics.**
981 **Supplementary Table 8. Non-SCR events identified in rice by proteogenomics.**
982 **Supplementary Table 9. SCR events identified in soybean by proteogenomics.**
983 **Supplementary Table 10. Non-SCR events identified in soybean by**
984 **proteogenomics.**
985 **Supplementary Table 11. SCR events identified in *Arabidopsis* by proteogenomics.**
986 **Supplementary Table 12. Non-SCR events identified in *Arabidopsis* by**
987 **proteogenomics.**
988 **Supplementary Table 13. Functional signals predicted in C-terminal extensions**
989 **of maize SCR events.**

990 **Supplementary Table 14. Primers used in this study.**

991

992 **Supplementary Dataset 1: Motifs predicted by Tomtom in the C-terminal**

993 **extensions of SCR transcripts in maize.**